A Robotic Manipulator Using Dual-Motor Joints: Prototype Design and Anti-Backlash Control

Jiqian Xu, Huaizhen Wang, Qiankun Zhao, Yue Gao, Yingcai Wan, and Lijin Fang

***Abstract*—This letter focuses on the design and control of a novel seven-degree-of-freedom (7-DOF) robotic manipulator (D-Arm) to address the issue of backlash nonlinearity coupling unknown disturbance through the dual-motor anti-backlash control technology. Specifically, the first three axes of the D-Arm near the base are implemented as dual-motor joints (DMJs), while the remaining four axes are single-motor joints (SMJs), which achieve a more comprehensive performance. For DMJs, as over-actuated systems, we first discover an internal disturbance phenomenon named servo-conflict and consider it in the controller design. To mitigate the adverse effects of backlash coupling disturbance, an admittance control-based position compensator is proposed. Then, after the backlash elimination, a dual-motor linear active disturbance rejection controller is effectively developed for load tracking task of the DMJ. In the presence of unknown backlash and disturbance, the proposed strategy can improve both transient and steady-state position tracking response, reduce energy consumption without requiring any backlash model information. The effectiveness and simplicity of the developed control strategy are verified through comparative experiments on the D-Arm.**

***Index Terms*—Motion control, redundant robots, dual-motor joints, over-actuated systems, anti-backlash control.**

I. Introduction

ROBOTIC manipulators are increasingly becoming essential elements of the modern industry and social life, where they assist humans or cooperate with them hand-in-hand in many tasks, such as handling [1], assembly [2], machining [3], surgery [4]. However, robotic manipulators as geared mechanical systems, always in acceleration and deceleration, are inevitably affected by the gear backlash. The backlash coupling disturbance, degrades the transmission accuracy and tracking performance and further aggravates the mechanical wear. Anti-backlash strategies can be divided into two categories according to different mechanisms: ***mechanical*** and ***electrical*** anti-backlash.

Mechanical anti-backlash technology involves the use of mechanical components to reduce or eliminate backlash. One of the most common methods is to use preloading spring which can be found in many off-the-shelf productions, such as KG anti-backlash spur gears, Zahnradfertigung OTT worm gears, and THK double nut ball screws. These mechanisms apply a force to the gear teeth, which eliminates the clearance between the teeth and reduces backlash. However, due to their structure and volume, these technologies have not been widely used in the field of robotics. In addition, strain wave gearboxes rely on the elastic mechanics of metals to realize the zero-backlash transmission, leading to the large-scale application in the field of robotics [5]. Although the mechanical anti-backlash technology has been widely applied in many fields, it must be acknowledged that it has shortcomings such as complex structure, inflexible backlash adjustment, and difficult maintenance.

To reduce the effect of backlash and guarantee system performance with the single-motor drive, various control methods have been proposed, such as switched damping control [6], shaft torque compensator-based shaft torque limiting control [7], smooth backlash inverse model-based compensation [8], linear active disturbance rejection control (LADRC) [9] and model predictive control [10]. Unfortunately, single-motor anti-backlash controllers are derived from feedback control theory, which only allows them to correct the control command of the actuator after backlash has already affected the system. This is a passive anti-backlash control strategy that can only estimate and compensate backlash within a relatively small control bandwidth range. The parameters of the controller must be carefully tuned to balance stationarity and rapidity of backlash traversing, which may not meet the requirements for high dynamic response of robots in some application scenarios.

The dual-motor anti-backlash technology is an active (feedforward) control strategy that shows great potential in mitigating the adverse effects of backlash. In industrial field, SIEMENS successfully integrated the dual-motor anti-backlash controller (named as master-slave coupling) in SINUMERIK 840D sl CNC system. The high-gain nonlinearity compensator [11] used to reduce backlash in dual-motor driving systems requires a large peak motor torque and results in gear tooth collisions during meshing, limiting its effectiveness. In [12] a switching dual-motor anti-backlash strategy has been proposed to increase

Manuscript received 6 June 2023; accepted 1 October 2023. Date of publication 27 October 2023; date of current version 6 November 2023. This letter was recommended for publication by Associate Editor P. Di Lillo and Editor C. Gosselin upon evaluation of the reviewers' comments. This work was supported in part by the National Natural Science Foundation of China under Grant 62273081, in part by the Natural Science Foundation of Liaoning Province under Grant 2022JH2/101300202, in part by the Science and Technology Small and Medium Enterprises Innovation Ability Enhancement Project of Shandong Province under Grant 2023TSGC0226, and in part by the Key R&D Plan of Shandong Province (Competitive Innovation Platform) under Grant 2023CXPT094. *(Corresponding author: Lijin Fang.)*

Jiqian Xu, Qiankun Zhao, Yue Gao, Yingcai Wan, and Lijin Fang are with the Faculty of Robot Science and Engineering, Northeastern University, Shenyang 110819, China (e-mail: jiqian_xu@qq.com; robokun@qq.com; imgaoyue@163.com; wyc_rt@163.com; ljfang@mail.neu.edu.cn).

Huaizhen Wang is with the Institute of Shandong New Generation Information Industry Technology, Inspur group, Jinan 250101, China (e-mail: whz1228@163.com).

Digital Object Identifier 10.1109/LRA.2023.3327867

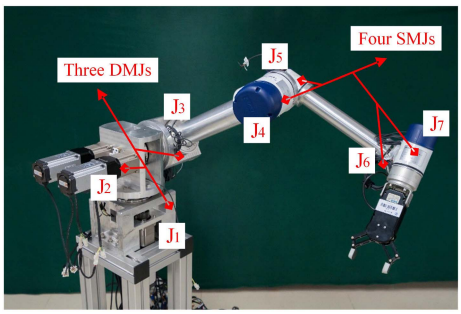

Fig. 1. Prototype diagram of the developed D-Arm. The first three joints near the base are equipped with DMJs ($J_1 \sim J_3$), and the remaining four joints close to the end-effector are equipped with SMJs ($J_4 \sim J_7$).

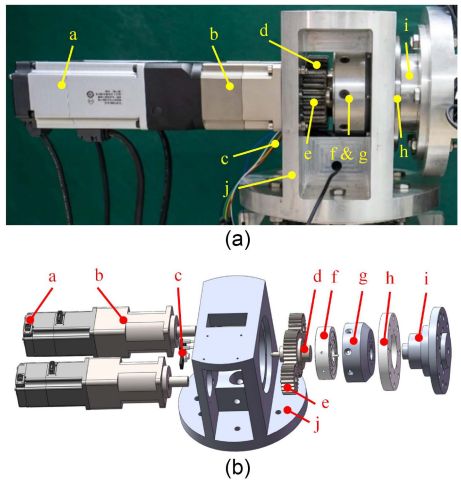

Fig. 2. Prototype and CAD explosion view of the DMJ. (A) Prototype diagram of the developed DMJ; (B) CAD explosion diagram of the developed DMJ: (a) Permanent magnet synchronous motor. (b) Planetary gearbox. (c) Load-side single-turn absolute encoder. (d) Load gear. (e) Pinion. (f) Torque sensor. (g) Coupling flange. (h) Cross roller bearing. (i) Output shaft. (j) Support.

stiffness and reduce backlash for a parallel kinematic manipulator. Nevertheless, the strategy can only ensure the anti-backlash performance at initial and final positions. Other researchers [13], [14] utilized a constant bias torque dual-motor anti-backlash strategy to enhance the control performance for dual-motor driving system. However, the coupling between backlash and disturbance is not considered in existing strategies, which means that the bias torque setting must involve a trade-off between energy consumption and anti-backlash control performance.

In summary, existing mechanical structures and control methods unfortunately still remain challenges in efficiently eliminating gear backlash coupling unknown disturbance. Therefore, in this work, following the dual-motor anti-backlash theory, we are dedicated to design both a seven-degree-of-freedom (7-DOF) serial type robotic manipulator and a dual-motor anti-backlash controller with the aim of addressing the limitations of the aforementioned approaches. This work provides a new approach for backlash reduction in the field of robotics. The main contributions of this work are as follows:

- A novel 7-DOF robotic manipulator consisting of three dual-motor joints (DMJs, $J_1 \sim J_3$) and four single-motor joints (SMJs, $J_4 \sim J_7$) is designed and manufactured.
- We first discover an internal disturbance phenomenon named servo-conflict on the dual-motor driving system and consider it in the controller design.
- To deal with backlash and unknown external and internal disturbance, we propose an admittance control-based position compensator combined with LADRC position tracking controller for DMJs, without requiring any backlash model information.
- Experiments show that our method improves both transient and steady-state position tracking response, reduces energy consumption, and achieves a positioning repeatability of ± 0.05 mm for the D-Arm following ISO 9283:1998.

II. Mechanics of the D-Arm

The prototype and CAD explosion diagram of the DMJ are presented in Fig. 2. There are two drivetrains, each of which consists of a servo motor from Panasonic (A6 MHMF042) with a rated torque of $1.27\,\mathrm{Nm}$ and planetary gearbox from NEWGEAR (PD60) with a reduction ratio of 50:1. Compared to other robotic gearbox solutions, the planetary gearbox has the best efficiency (above 90%), affordability and the no-load starting torque is very low, but its backlash is also the largest ($4 \sim 9$ arcmin) [5]. Fortunately, enhanced by the dual-motor anti-backlash technology, its shortcoming about backlash could be overcome. An anti-backlash unit consists of dual pinions coupled to the two drivetrains, respectively, and a load gear coupled to the output shaft. Three gears of the anti-backlash unit are purchased from MiSUMi (GEAKB2.0) with a reduction ratio of 33:25. Hence, the total system reduction ratio is 66. The platform is equipped with three encoders and one torque sensor. Specifically, two multi-turn absolute encoders (resolution: 23 b) are installed on the motor side, which are used for state feedback control. One single-turn absolute encoder (resolution: 19 b) from ZeroErr (eCoder20) is mounted on the load side. The output torque provided by the dual-motor is monitored by a torque sensor from SUNRISE INSTRUMENTS (M2210 C) with a rated capacity of $100\,\mathrm{Nm}$. Additionally, it can be easily designed in a form with a hollow hole for cable placement.

The developed D-Arm is a redundant 7-DOF serial-type robot, and the prototype of it is shown in Fig. 1. It has the same configuration as the Rethink Sawyer and the maximum work reach is around $900\,\mathrm{mm}$. The theoretical payload of the robot is $12\,\mathrm{kg}$. Although DMJs have many advantages, their shortcomings in volume and weight cannot be ignored. Hence, we introduce a more balanced solution for robot joint design: Compared to normal robotic manipulators, the significant difference is that it consists of three DMJs and four traditional SMJs with strain wave gearboxes. In our opinion, for this type of robot, the design standards of robotic joints are different. It can be divided into two groups. One group includes three joints ($J_1 \sim J_3$), which are near the base. Their inertia and gravity have a relatively limited influence on the robot. However, the requirements for accuracy, stiffness, capacity, and robustness of these joints are very high. Therefore, the DMJ is particularly suitable for this kind of joint.

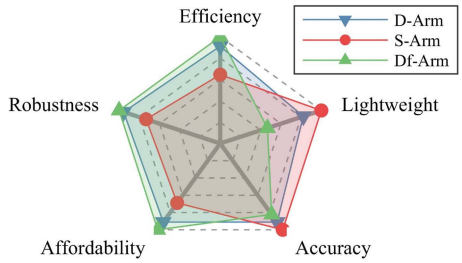

Fig. 3. Estimated performance comparison of different joint implementations of the serial-type robot. The scores for each index are relative, and the data comes from [5] and our experience. Here, the S-Arm represents the serial-type robot only equipped with SMJs, and the Df-Arm represents that all of joints are DMJs. Although the other two solutions have more clearly defined strengths and weaknesses, the proposed D-Arm offers a more balanced performance.

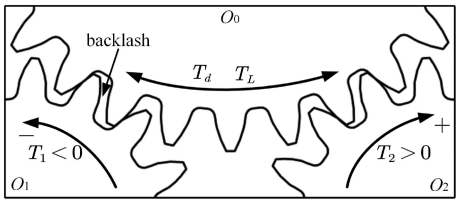

Fig. 4. Schematic diagram of the DMJ system. Here, O_1 and O_2 represent dual pinion coupled to dual driving motor, respectively, and O_0 represents load gear coupled to driven load.

The other group includes the remaining joints ($J_4 \sim J_7$) with opposite design standards. The performance of a serial-type robot is very sensitive to their inertia and gravity. The strain wave gearbox is distinguished by its larger diameters than lengths, resulting in lower weight compared to other gear train transmission technologies. This design yields the best torque-to-weight ratios [5]. Undoubtedly, these advantages make the SMJ a better suit for the joint closer to the end-effector. The four SMJs of the D-Arm are manufactured by SIASUN, and their model numbers are RjM25 (J_4) and RjM14 ($J_5 \sim J_7$), respectively. In conclusion, the joint design of the D-Arm is an attempt to address trade-offs between a number of design standards, i.e., accuracy, efficiency, lightweight, affordability, robustness. Fig. 3 shows the estimated performance comparison of different joint implementations of the serial-type robot. From Fig. 3, we can see that the proposed D-Arm has a more balanced performance. It is worth mentioning that, inspired by the scale optimization method proposed in [15], we can further compensate for the drawbacks of DMJs in terms of volume and weight. In the future, we plan to conduct in-depth research on this issue.

III. Control-Oriented Model Approximation for the DMJ

A schematic diagram of the DMJ system is presented in Fig. 4. Here, O_1 and O_2 represent two pinions coupled to two driving motors that cooperatively mesh with the load gear labeled as O_0 connected to the driven load. This system can be modeled as

$$\begin{cases} J_L\dot{\omega}_L + b_L\dot{q}_L + T_d = \sum_{i=1}^{2} T_{s,i} \\ J_m\dot{\omega}_i + b_m\dot{q}_i = T_i - T_{s,i}/r, \quad i = 1,2 \end{cases} \tag{1}$$

where the subscript $i = 1, 2$ represents the number of the dual driving motor (M1, M2); J_L and J_m are the inertia moment of the load and single-motor, respectively; q_L and q_i are the angular position of load and dual-motor, respectively; ω_L and ω_i denote the angular speed of load and dual-motor, respectively; b_L and b_m are the load- and motor-side viscous friction coefficient, respectively; r is the total system reduction ratio ($r = 66$); T_i denotes the command torque of dual-motor; T_d indicates the external disturbance, i.e., the external torque applied to the joint due to gravity or the environment; $T_{s,i}$ is the geartrain transmission torque produced by dual-motor. Ordinarily, the transmission torque $T_{s,i}$ is established through the dead-zone model [16].

$$T_{s,i} = \begin{cases} k_s\left(\Delta q_i - q_b\right) + c_s\Delta\dot{q}_i & \Delta q_i > q_b \\ 0 & -q_b \leqslant \Delta q_i \leqslant q_b \\ k_s\left(\Delta q_i + q_b\right) + c_s\Delta\dot{q}_i & \Delta q_i < -q_b \end{cases} \tag{2}$$

where $\Delta q_i = q_i/r - q_L$ and q_b is the backlash width; b_s and k_s denote the internal damping and stiffness coefficient, respectively. From the dead-zone model, we can conclude that the nonlinearity of $T_{s,i}$ is mainly caused by backlash.

The reality is that modeling backlash accurately using the dead-zone model is challenging due to the strong nonlinearity associated with it [17]. Dual-motor anti-backlash control is an electronically preloading anti-backlash strategy that utilizes two motor/gearbox assemblies with dual pinion operating on the same load gear (output shaft). One pinion drives the axis, while the secondary pinion is preloaded to eliminate backlash without requiring any backlash model information.

If it is successful to implement the dual-motor anti-backlash control strategy, there is no backlash in this system. Hence, the dynamics of the transmission torque $T_{s,i}$ could be ignored in the backlash-free state, i.e., $q_1 = q_2$ and $q_i/r = q_L$ are satisfied. Then, we can reconstruct (1) by eliminating $T_{s,i}$ as follows:

$$\begin{cases} T_L + T_d/r = T_1 + T_2 \\ (J_L/r^2 + 2J_m)\dot{\omega}_1 + (b_L/r^2 + 2b_m)\dot{q}_1 = T_L \end{cases} \tag{3}$$

where T_L is the equivalent load torque. The lumped disturbance (including external and internal disturbance, unmodeled dynamics) is defined as follows:

$$\begin{aligned} \boldsymbol{f} &= \begin{bmatrix} f_1 & f_2 \end{bmatrix}^{\mathrm{T}} \\ &= \begin{bmatrix} b_o(T_{u,1} - b_u\omega_1) & b_o(T_{u,2} - b_u\omega_2) \end{bmatrix}^{\mathrm{T}} \end{aligned} \tag{4}$$

where the subscript $g = 1, 2$, $g \neq i$, $b_o = 1/(J_L/r^2 + 2J_m)$, $b_u = b_L/r^2 + 2b_m$, and $T_{u,i} = T_g - T_d/r$. Moreover, assume that $\boldsymbol{f}$ is differentiable [9] and let $\boldsymbol{h} = [0 \quad 0 \quad \dot{f}_1 \quad 0 \quad 0 \quad \dot{f}_2]^{\mathrm{T}}$. Then, reconstruct (3) in an extended state-space equation form as follows:

$$\begin{cases} \dot{\boldsymbol{x}} = \boldsymbol{A}\boldsymbol{x} + \boldsymbol{\Gamma}\boldsymbol{u} + \boldsymbol{h} \\ \boldsymbol{y} = \boldsymbol{C}\boldsymbol{x} \end{cases} \tag{5}$$

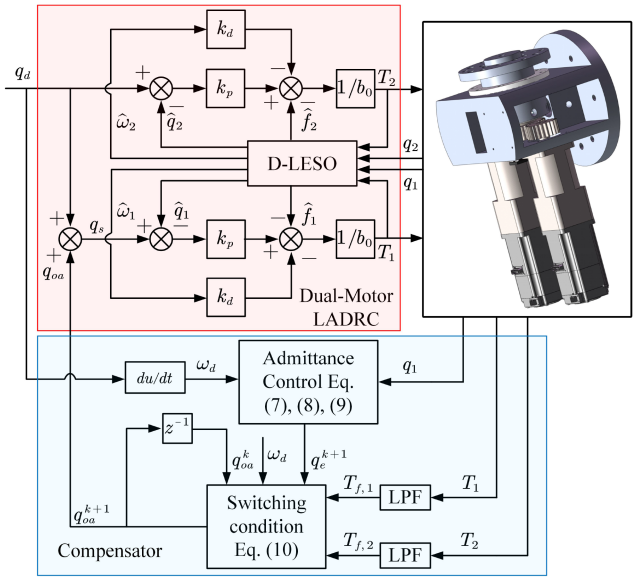

Fig. 5. Block scheme of the developed dual-motor LADRC anti-backlash controller for the DMJ.

where the system states $\boldsymbol{x} = [q_1 \quad \omega_1 \quad f_1 \quad q_2 \quad \omega_2 \quad f_2]^{\mathrm{T}}$, the control input $\boldsymbol{u} = [T_1 \quad T_2]^{\mathrm{T}}$, and the matrix $\boldsymbol{A}$, $\boldsymbol{\Gamma}$, $\boldsymbol{C}$ are:

$$\begin{aligned} \boldsymbol{A} &= \begin{bmatrix} 0 & 1 & 0 & 0 & 0 & 0 \\ 0 & 0 & 1 & 0 & 0 & 0 \\ 0 & 0 & 0 & 0 & 0 & 0 \\ 0 & 0 & 0 & 0 & 1 & 0 \\ 0 & 0 & 0 & 0 & 0 & 1 \\ 0 & 0 & 0 & 0 & 0 & 0 \end{bmatrix} \\ \boldsymbol{\Gamma} &= \begin{bmatrix} 0 & 0 & 0 & 0 & b_o & 0 \\ 0 & b_o & 0 & 0 & 0 & 0 \end{bmatrix}^{\mathrm{T}} \\ \boldsymbol{C} &= \begin{bmatrix} 1 & 0 & 0 & 0 & 0 & 0 \\ 0 & 0 & 0 & 1 & 0 & 0 \end{bmatrix} \end{aligned} \tag{6}$$

In the following section, an adaptive position compensator is proposed to deal with the gear backlash, so that the DMJ system can always be kept in the backlash-free state modeled by (5). Then, based on this backlash-free model, the position tracking controller of this system can be conveniently designed under the LADRC controller framework.

IV. Controller Design

The aim of this study is to achieve better control performance through a simple controller. Fig. 5 illustrates the proposed dual-motor LADRC anti-backlash controller for the DMJ. The developed controller consists of an admittance control-based position compensator and a dual-motor LADRC position controller. In this paper, we only consider the motor-side position information, which is the most common configuration in the field of robotics. The motor-side encoder of M2 is chosen as the position feedback signal, and both motors always operate in semi-loop position control mode. Compared to the M2, the position compensator is implemented to dynamically modify the position reference of M1.

A. Position Compensator for Anti-Backlash

The dual-motor anti-backlash control should ensure the performance of eliminating backlash while reducing energy consumption as much as possible in the presence of the external disturbance. Specifically, when the external disturbance occurs, it is necessary to actively change the torque of dual-motor to ensure that the load gear will not lose contact with the pinion. In other cases, to improve the energy efficiency, the preloading torque of dual-motor should be maintained at a relatively low level. There are two solutions producing a reasonable preloading torque of dual-motor.

Solution A: Let the M1 work in the torque control mode and track a constant torque reference and the M2 is implemented with the position control mode to track the desired position [13]. This solution can induce the desired preloading torque, but if the external disturbance T_d exceeds the desired preloading torque, which can cause loss of contact between the pinion coupled to the M2 and the load gear.

Solution B: Set the dual-motor to position control mode and two motors are implemented to track the same target position individually and add an appropriate compensation to the position reference fed to the M1, named constant position compensator-based anti-backlash controller (CPC) [12]. Ideally, the preloading torque is constantly produced by the constant position compensation at different positions. When the external disturbance is presented, based on this control strategy, the torque of the dual-motor is actively changed to reject it because of the best anti-disturbance performance of the position control mode. Therefore, this solution has the best performance in rejecting the external disturbance to protect the engagement between gears. It seems to be a perfect solution for this problem. Unfortunately, the DMJ is a kind of over-actuated system. In real gear trains, there are unavoidable manufacturing and assembly errors, which will induce the preloading torque variable and hence induce unnecessary waste of energy or anti-backlash failure. This is an internal disturbance phenomenon named ***servo-conflict***. See Section V-A for more details.

The drawback of the above-mentioned anti-backlash solutions can be overcome by the following adaptive position compensator. When encountering the servo-conflict, the M1 should be set to control contact force (by the dynamic position compensation strategy) between the pinion and the load gear (FC mode); in the other situations, to contract the external disturbance, the M1 should be set to position control (by the constant position compensation strategy) for obtaining engagement between gears (PC mode). In this paper, the admittance control is selected as a contact force control strategy to design the position compensator due to its perfect compatibility with the position control mode. To this end, an admittance control-based position compensator is proposed, shown in Fig. 5.

1) Contact Force Control Mode (FC Mode): The admittance control is represented by:

$$B\dot{q}_e + Kq_e = T_h - T_c \tag{7}$$

where K and B are the desired stiffness and damping coefficient, respectively; $q_e = q_d - q_1$ and q_d is the joint position reference;

T_h is the desired preloading torque. Generally, it is $5\% \sim 15\%$ of the rated torque of a driving motor (T_{rat}), i.e., $T_h = 0.05T_{rat} \sim 0.15T_{rat}$; T_c is the filtered motor torque. Following the direction of the desired speed ω_d, T_h and T_c are designed as:

$$T_h = \begin{cases} -0.1T_{rat} & \text{if } \omega_d \geqslant 0 \\ 0.1T_{rat} & \text{if } \omega_d < 0 \end{cases}$$

$$T_c = \begin{cases} T_{f,1} & \text{if } \omega_d \geqslant 0 \\ T_{f,2} & \text{if } \omega_d < 0 \end{cases} \tag{8}$$

where $T_{f,1}$ and $T_{f,2}$ are the motor torque of M1 and M2, respectively, which are filtered by the second-order low-pass filter (LPF). Therefore, based on (7) and (8), the output of the admittance control can be given as follows.

$$\begin{cases} q_e^k = q_d^k - q_1^k \\ \dot{q}_e^{k+1} = \left(T_h - T_c - Kq_e^k\right)/B \\ q_e^{k+1} = q_e^k + \dot{q}_e^{k+1} t_s \end{cases} \tag{9}$$

where t_s is the sample time and q_e^{k+1} is the compensation for the position reference computed by the admittance control at $(k+1)t_s$.

2) Pure Position Control Mode (PC Mode): In the PC mode, the position compensation at current sample time is the same as the last sample time (i.e., the position compensation is unchangeable, see (10)). The position control action is purposefully made stiff to ensure tracking of the desired position and to enhance disturbance rejection.

3) Switching Condition: The disturbance torque and load torque could not be estimated properly in the existence of the servo-conflict since the influence of them on the torque of dual-motor is coupled (see (3)). In this paper, we support another perspective that the proposed principle of anti-backlash control strategy is indirectly implemented by assessing the torque of dual-motor.

To balance the rejection of disturbance and energy consumption, the whole movement of the DMJ is dived into PC mode and FC mode. To determine the activation of the control mode in a reasonable manner, a switching condition is designed in terms of the filtered dual-motor torque $T_{f,i}$ and desired speed ω_d as follows:

$$q_{oa}^{k+1} = \begin{cases} \text{if } T_{f,2} > T_{tu}, \\ q_e^{k+1} \text{or } T_{f,1} > -T_{tl}, \quad \text{(FC mode)} \\ \text{and } \omega_d \geqslant 0; \\ \text{if } T_{f,2} < T_{tl}, \\ q_e^{k+1} \text{or } T_{f,1} < -T_{tu}, \quad \text{(FC mode)} \\ \text{and } \omega_d < 0; \\ q_{oa}^k \quad \text{else.} \qquad \text{(PC mode)} \end{cases} \tag{10}$$

where q_{oa}^{k+1} is ultimate position compensation determined at $(k+1)t_s$; T_{tl} and T_{tu} are the lower and upper threshold dual-motor torque for the switching condition, respectively, and $T_{tu} > |T_h| > T_{tl}$ is satisfied. The following will explain the design principle of the T_{tu} and T_{tl}.

If the pinion is disengaged with the load gear (backlash phase), the driving motor turns around without load. In this situation, a small motor torque can produce a large acceleration. It is assumed that the torque T_{tu} can accelerate the motor without load from the station to the rated speed within a short time period ($\Delta t < 1$ s), and the load speed is much less than the rated speed and will not change much during this period normally. Consequently, it is concluded that if the motor torque is greater than T_{tu} ($|T_{f,i}| > T_{tu}$), the engagement situation between gears could be achieved (contact phase). Hence, the load-side position information can be obtained through the motor-side encoder. Likewise, if the motor torque is lower than T_{tl} (i.e., $|T_{f,i}| < T_{tl}$), it may enter the backlash phase. Through our repeated testing, selecting $T_{tu} = 0.2T_{rat}$, $T_{tl} = 0.08T_{rat}$ is more reasonable considering the trade-off between the energy consumption and anti-backlash performance. Therefore, by utilizing the proposed switching condition in (10), it becomes possible to determine the working mode of the dual-motor (either PC or FC mode) based on the desired speed ω_d and dual-motor torque $T_{f,i}$, without knowing which specific factors (the external disturbance, servo-conflict or load torque) lead to.

Finally, the command position of the M1 is given by:

$$q_s^{k+1} = q_d^{k+1} + q_{oa}^{k+1} \tag{11}$$

where q_d^{k+1} and q_s^{k+1} are the position reference of M2 and M1 at $(k+1)t_s$, respectively.

The above analyses indicate that the proposed method can effectively tackle the anti-backlash problem while considering unknown disturbance, and it also optimizes energy consumption. Additionally, the method operates without requiring any backlash model information.

B. Position Tracking Controller

Based on the above analysis, once the proposed adaptive position compensator is successfully implemented, the DMJ system will remain in the backlash-free status modeled by (5). Inheriting from the LADRC framework [9], we constructed a dual-motor liner extended state observer (D-LESO) to estimate the states of the system modeled by (5) as follows.

$$\begin{cases} \dot{\hat{\boldsymbol{x}}} = \boldsymbol{A}\hat{\boldsymbol{x}} + \boldsymbol{\Gamma}\boldsymbol{u} + \boldsymbol{L}\left(\boldsymbol{y} - \hat{\boldsymbol{y}}\right) \\ \hat{\boldsymbol{y}} = \boldsymbol{C}\hat{\boldsymbol{x}} \end{cases} \tag{12}$$

where $\hat{\boldsymbol{x}} = [\hat{q}_1 \quad \hat{\omega}_1 \quad \hat{f}_1 \quad \hat{q}_2 \quad \hat{\omega}_2 \quad \hat{f}_2]$ denotes the estimation for the system states $\boldsymbol{x}$; $\boldsymbol{L}$ is the observer gain vector

$$\boldsymbol{L} = \begin{bmatrix} \beta_1 & \beta_2 & \beta_3 & 0 & 0 & 0 \\ 0 & 0 & 0 & \beta_4 & \beta_5 & \beta_6 \end{bmatrix} \tag{13}$$

Finally, following the estimated states, the dual-motor LADRC feedback law for position tracking tasks can be designed as:

$$\begin{bmatrix} T_1 \\ T_2 \end{bmatrix} = \frac{k_p}{b_o}\left(\begin{bmatrix} q_d \\ q_s \end{bmatrix} - \begin{bmatrix} \hat{q}_2 \\ \hat{q}_1 \end{bmatrix}\right) - \frac{k_d}{b_o}\begin{bmatrix} \hat{\omega}_2 \\ \hat{\omega}_1 \end{bmatrix} - \frac{1}{b_o}\begin{bmatrix} \hat{f}_2 \\ \hat{f}_1 \end{bmatrix} \tag{14}$$

where k_p and k_d are the controller gain; q_d and q_s are the position reference of M2 and M1, respectively. It can be concluded that once the system model is specifically formulated as shown in (5), the position tracking problem can be effectively solved within the LADRC framework.

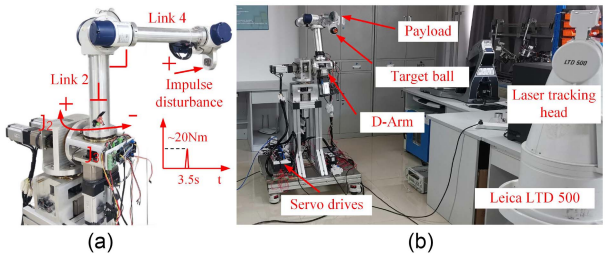

Fig. 6. Test bench for (A) position tracking response of the DMJ and (B) positioning repeatability assessment of the D-Arm.

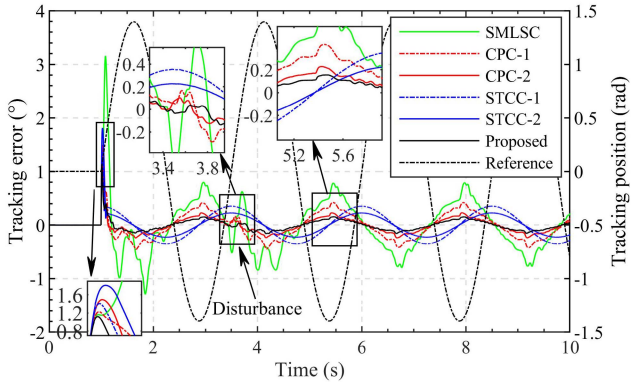

Fig. 7. Tracking error and position profiles of different controllers.

V. Experimental Results and Discussion

The experimental setup is depicted in Fig. 6. The control software runs on a desktop PC (upper controller) with an Ubuntu 18.04 LTS distribution patched with PREEMPT_ RT (4.4.139-rt192). To facilitate control information exchange with the D-Arm, an open-source Linux-based EtherCAT master stack IgH is employed. The position reference trajectory and proposed control strategy are computed online on the desktop PC with a sample time t_s of 1 ms. All units presented in the results are converted to load-side units, considering the reduction ratio ($r = 66$).

The single-motor LADRC semi-loop control (SMLSC) [9], the dual-motor LADRC anti-backlash control with constant position compensation (CPC) [12] and the speed/torque coupling dual-motor anti-backlash control (STCC) proposed by SIEMENS were used as benchmarks to facilitate performance evaluation. The motor-side encoder of the M2 of each DMJ joint was selected as the joint position feedback signal. For a fair comparison, the LADRC parameters of SMLSC, CPC, and proposed controller were the same. By the trial-and-error method, the control parameters of LADRC controller and PID controller of STCC are tuned considering tracking accuracy and robustness.

The parameters of LADRC were specified as $\beta_1 = \beta_4 = 720$, $\beta_2 = \beta_5 = 172800, \beta_3 = \beta_6 = 1382400, k_p = 2500, k_d = 100$, $b_o = 4200$. For the STCC, the position gain, speed gain, speed integral gain, preloading torque gain, and preloading torque integral gain were 130, 130, 25, 130, 120, respectively. We conducted two different sets of experiments on the STCC and CPC based on different preloading torques. *Case* 1 (CPC-1, STCC-1): The preloading torque was selected as $0.1T_{rat}$. *Case* 2 (CPC-2, STCC-2): The preloading torque was designed as $0.3T_{rat}$. The parameters of the proposed controller were $K = 0.002$, $B = 1$, $T_{tu} = 0.2T_{rat}, T_{tl} = 0.08T_{rat}$. In the FC mode of the proposed controller, the cutoff frequency of LPF was set to 100 Hz.

A. Position Tracking Response of the DMJ

The pose of the robot during this experiment is shown in Fig. 6(a).The J_3 of the D-Arm was used as the test bench, equipped only with a flywheel-type load whose moment of inertia is $1.05\,\mathrm{kg\,m^2}$ (the more distal parts of the robot). The flywheel-type load was obtained by locking the link 2 in the vertical position and link 4 in the horizontal position. The sinusoidal signal $q_d = 4\pi/9\sin(0.8\pi t)$ was used as the desired tracking trajectory shown in Fig. 7. An impulse disturbance (about 20 Nm) with the same direction of movement is manually performed to the end of D-Arm at about 3.5 s. The disturbance in this direction can more easily excite the backlash of the system. During the experiment, the maximum speed that J_3 can achieve is $201\,^\circ/\mathrm{s}$ and the maximum output torque is $38.7\,\mathrm{Nm}$ after 5 s (at steady tracking state). As a comparison, the nominal speed of J_3 is $180\,^\circ/\mathrm{s}$ and the nominal output torque is $70\,\mathrm{Nm}$ at anti-backlash control mode. The backlash width of this joint is approximately 0.7°. The tracking error $q_c = q_d - q_2$ of these controllers is shown in Fig. 7. Comprehensive comparisons of the response performance of those control algorithms are depicted in Table I, where the experimental results (from time $t = 0$s to $t = 10$s) are summarized with respect to four indices, which are the maximum absolute error (i.e., MAE $= \max[|q_c(t)|]$), and the integral absolute error (i.e., IAE $= \int |q_c(t)|\mathrm{d}t$), the integral time absolute error (i.e., ITAE $= \int t|q_c(t)|\mathrm{d}t$), and the integral square error (i.e., ISDE $= \int (q_c(t) - \bar{q_c})^2\mathrm{d}t$) for the mean value $\bar{q_c}$ of the tracking error q_c.

TABLE I
Tracking Comparison for Different Controllers

Indices	Proposed	SMLSC	CPC-1	CPC-2	STCC-1	STCC-2
MAE	1.12	3.16	1.23	1.49	1.41	1.81
IAE	0.73	3.72	1.98	1.06	2.08	1.39
ITAE	1.72	18.44	10.37	5.47	2.85	1.85
ISDE	0.10	2.55	0.59	0.22	0.62	0.37
EC	180.70	79.27	141.57	236.08	109.97	261.17

In Fig. 7 and Table I, it could be concluded that the SMLSC tracking performance is the poorest, particularly in the initial movement stage, the reverse movement stage, or when the system is subject to disturbance. Causing the gear meshing teeth to separate in those stages, which increases the uncertainty of the system and further slashes the response bandwidth of this controller. Normally, the backlash is regarded as the uncertainty/disturbance in the single-motor control scheme (e.g., the SMLSC). Under limited observation and control bandwidth, there is not enough information to accurately and immediately reconstruct it. In particular, when the backlash occurs, the pinion must go through the backlash to rebuild the engagement with

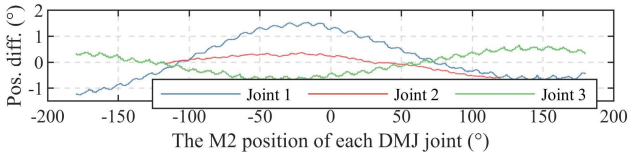

Fig. 8. Position difference between the dual-motor of three DMJs. Here, the position difference $q_{\Delta,k}$ is variable, and $q_{\Delta,k}$ ranges of each DMJ joint are $-1.4^\circ < q_{\Delta,1} < 1.5^\circ$, $-0.6^\circ < q_{\Delta,2} < 0.4^\circ$, $-0.7^\circ < q_{\Delta,3} < 0.6^\circ$, respectively.

the load gear. Hence, it is a physical limitation that inevitably induces impact and delay. Such drawbacks are intrinsic for the single-motor control scheme when the system has a non-negligible backlash.

According to Table I, compared to the SMLSC, there are relatively small indices for these dual-motor control methods considering the gear backlash and external disturbance. Among these control algorithms, the proposed controller can achieve the highest tracking performance. Specifically, the proposed controller gives the smallest MAE, IAE, and ITAE indices, indicating that it has the smallest tracking error throughout the experimental phase. In addition, from the perspective of transient performance, the proposed controller also keeps the smallest ISDE, which indicates that the best transient tracking performance (i.e., the least oscillation and overshoot) is also obtained. The proposed dual-motor control scheme can be regarded as a feedforward anti-backlash control strategy. In other words, when the backlash is about to occur, it will be eliminated instantly. Therefore, a considerable improvement in tracking performance could be achieved, even though the construction and parameters of the position controller are the same as those of the single-motor control scheme.

Furthermore, the CPC and STCC eliminate the backlash incompletely (leading to four indices greater than the proposed controller) because the servo-conflict is not considered. The position difference between two motors of three DMJs is presented in Fig. 8. The M2 of each DMJ joint is set to position control mode with a variation of the position reference from negative limit to positive limit (J_1 and J_3: $[-180^\circ\ 180^\circ]$, J_2: $[-120^\circ\ 120^\circ]$) with uniform speed, while the M1 of each joint is set to torque control mode with a constant preloading torque reference (i.e., $T_1 = -0.1T_{rat}$). We simultaneously record the position of two motors and compute the difference $q_{\Delta,k} = q_{2,k} - q_{1,k}$, where the subscript $k = 1, 2, 3$ is the joint number. Ideally, $q_{\Delta,k}$ is close to a constant. However, according to Fig. 8, $q_{\Delta,k}$ is variable, and the range of $q_{\Delta,k}$ is different with respect to different joints (i.e., $-1.4^\circ < q_{\Delta,1} < 1.5^\circ$, $-0.6^\circ < q_{\Delta,2} < 0.4^\circ$, $-0.7^\circ < q_{\Delta,3} < 0.6^\circ$). This phenomenon is mainly caused by unavoidable manufacturing and assembly errors of the mechanic system. For STCC and CPC, variable $q_{\Delta,k}$ can result in the given preloading torque not being correctly obtained during operation. Let's take J_3 as an example to further explain this issue. Assuming operation starts at 0° position of J_3, we will obtain a position compensation value $q^0_{\Delta,3}$ for M1 through the given preloading torque. From Fig. 8, it can be seen that when the joint runs at $-50^\circ < q_d < 0^\circ$, $q_{\Delta,3} < q^0_{\Delta,3}$ is satisfied, which

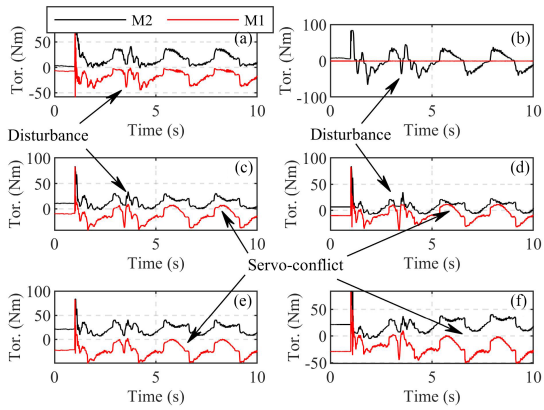

Fig. 9. Motor torque of different controllers. (A) Proposed controller; (B) SMLSC; (C) CPC-1; (D) STCC-1; (E) CPC-2; (F) STCC-2.

leads to the increase of the preloading torque and, therefore, to an unnecessary waste of energy; in other positions, $q_{\Delta,3} > q^0_{\Delta,3}$ is satisfied, which results in the decrease of the preloading torque and even the disengagement between the pinion and load gear (i.e., the backlash). Fig. 9 shows the motor torque of the four controllers, where the servo-conflict phenomenon is also clearly observed in the CPC and STCC. However, our proposed controller provides an adaptive compensation mechanism for tracking trajectory of M1, which greatly alleviates this problem. Therefore, the highest tracking performance can be achieved by the proposed controller.

Table I also displays the comparison subject to the energy consumption (EC) of each controller. It is quantified by EC $= \int |\dot{q}_d(t)|(|T_1(t)| + |T_2(t)|)\mathrm{d}t$ from time $t = 6$s to $t = 8.5$s. In summary, the conclusions drawn from Table I are: a) SMLSC exhibits the lowest energy consumption but the poorest tracking performance; b) STCC-2 and CPC-2 demonstrate relatively better tracking performance compared with STCC-1 and CPC-1, but they also have higher energy consumption due to the increase in preloading torque; c) Our proposed controller surpasses STCC-2 and CPC-2 in tracking performance while consuming less energy. Therefore, our proposed controller achieves the best control accuracy while attaining optimal energy efficiency.

B. Positioning Repeatability Assessment of the D-Arm

Fig. 6(b) displays the test bench that is deployed to measure the Positioning repeatability (PR) of the D-Arm with a Leica LTD 500 Laser Tracker (3D coordinate measurement repeatability: $\pm 2.5\,\mu\mathrm{m/m}$). The average distance between the target ball and the laser tracking head is $1.5\,\mathrm{m}$. Following ISO 9283:1998, at maximum rated load ($5\,\mathrm{kg}$ & anti-backlash control) and 200 mm/s speed on the inclined ISO test plane with five measured points named P1 $\sim$ P5 with 30 test cycles, the D-Arm is ordered to follow the target trajectory with all seven axes in motion.

Table II shows the PR performance of the D-Arm for each controller. From Table II, we can see that equipped with the proposed controller, the PR of the D-Arm is $\pm 0.05\,\mathrm{mm}$ better than that of the collaborative robotic manipulator (KUKA LBR

TABLE II
COMPARISON OF THE POSITIONING REPEATABILITY OF THE D-ARM FOR DIFFERENT CONTROLLERS

Target points	Proposed (mm)	CPC-1 (mm)	STCC-1 (mm)	SMLSC (mm)
P1	0.03	0.04	0.05	0.11
P2	0.04	0.03	0.048	0.08
P3	0.05	0.09	0.07	0.14
P4	0.03	0.08	0.05	0.13
P5	0.02	0.03	0.04	0.15
Max	0.05	0.09	0.07	0.15

iiwa ($7\,\mathrm{kg}$ & $800\,\mathrm{mm}$): $\pm 0.1\,\mathrm{mm}$), and worse than that of the industrial robotic manipulator (ABB IRB 1200 ($5\,\mathrm{kg}$ & $900\,\mathrm{mm}$): $\pm 0.025\,\mathrm{mm}$). Furthermore, from the measurement results in Table II, the PR of the SMLSC does not seem to be much inferior to that of our proposed controller. This is because the PR is less affected by backlash [18]. During the experiment, when the link 2 is in the vertically upright position, the direction of the total torque of J_2 (mainly influenced by gravity) will change, causing the load gear to cross the backlash and mesh with the opposite tooth surface of the driving gear (see Fig. 4). The same phenomenon also occurs on the J_1 and J_3, that is, the direction of the total joint torque is different from the direction of joint motion. This leads to motion discontinuities and impacts due to backlash, which can accelerate mechanical wear but less impact for short term static PR evaluation. However, the proposed strategy in this paper can effectively avoid this problem.

VI. CONCLUSION AND FUTURE WORKS

This letter presents a 7-DOF robotic manipulator that uses dual-motor anti-backlash control technology to deal with backlash nonlinearity coupling unknown disturbance. To acquire a more balanced performance, the first three joints of the D-Arm near the base are implemented as DMJs, while the rest four joints are SMJs. Under the assumption that the proposed dual-motor anti-backlash strategy can eliminate backlash efficiently, the nonlinear model of the dual-motor driving system is first transformed into a linear (backlash-free) model to facilitate the design of tracking controller. An internal disturbance phenomenon named servo-conflict is first discovered on the dual-motor driving system and considered it in the controller design. Considering backlash coupling unknown disturbance, an admittance control-based position compensator is proposed. Then, a dual-motor LADRC is developed for load tracking of the DMJ based on this linear model. The principle of the proposed strategy is to ensure the performance of eliminating backlash while reducing energy consumption as much as possible in the presence of unknown external disturbance and servo-conflict (internal disturbance). Unlike other dual-motor anti-backlash controllers, it works fine without requiring any backlash model information. The experimental results confirm that compared with other controllers, a) the improvement of transient and steady-state tracking response and reduction of energy consumption are achieved simultaneously for DMJs; b) following ISO 9283:1998, the ± 0.05 mm positioning repeatability of the D-Arm is obtained.

Nevertheless, the proposed control strategy exhibits certain constraints. It only effectively operates under the dual-motor preloading state. Therefore, as future work, it is necessary to find a way to optimize the driving torque of the dual-motor considering synchronous control.

REFERENCES

[1] K. Haninger, M. Radke, A. Vick, and J. Kruger, "Towards high-payload admittance control for manual guidance with environmental contact," *IEEE Robot. Automat. Lett.*, vol. 7, no. 2, pp. 4275–4282, Apr. 2022.

[2] A. Wan, J. Xu, H. Chen, S. Zhang, and K. Chen, "Optimal path planning and control of assembly robots for hard-measuring easy-deformation assemblies," *IEEE/ASME Trans. Mechatron.*, vol. 22, no. 4, pp. 1600–1609, Aug. 2017.

[3] W. Wang, Q. Guo, Z. Yang, Y. Jiang, and J. Xu, "A state-of-the-art review on robotic milling of complex parts with high efficiency and precision," *Robot. Comput.- Integr. Manuf.*, vol. 79, 2023, Art. no. 102436.

[4] T. Haidegger, "Autonomy for surgical robots: Concepts and paradigms," *IEEE Trans. Med. Robot. Bionics*, vol. 1, no. 2, pp. 65–76, May 2019.

[5] P. L. García, S. Crispel, E. Saerens, T. Verstraten, and D. Lefeber, "Compact gearboxes for modern robotics: A review," *Front. Robot. AI*, vol. 7, 2020, Art. no. 103.

[6] S. Yamada, M. Ruderman, and H. Fujimoto, "Piecewise affine (PWA) modeling and switched damping control of two-inertia systems with backlash," in *Proc. IEEE 15th Int. Workshop Adv. Motion Control*, 2018, pp. 479–484.

[7] M. Yang, C. Wang, D. Xu, W. Zheng, and X. Lang, "Shaft torque limiting control using shaft torque compensator for two-inertia elastic system with backlash," *IEEE/ASME Trans. Mechatron.*, vol. 21, no. 6, pp. 2902–2911, Dec. 2016.

[8] Z. Zhao, W. He, F. Zhang, C. Wang, and K.-S. Hong, "Deterministic learning from adaptive neural network control for a 2-DoF helicopter system with unknown backlash and model uncertainty," *IEEE Trans. Ind. Electron.*, vol. 70, no. 9, pp. 9379–9389, Sep. 2023.

[9] H. Zhang, S. Zhao, and Z. Gao, "An active disturbance rejection control solution for the two-mass-spring benchmark problem," in *Proc. Amer. Control Conf.*, 2016, pp. 1566–1571.

[10] A. Formentini, A. Oliveri, M. Marchesoni, and M. Storace, "A switched predictive controller for an electrical powertrain system with backlash," *IEEE Trans. Power Electron.*, vol. 32, no. 5, pp. 4036–4047, May 2017.

[11] T. Zeng, X. Ren, and Y. Zhang, "Fixed-time sliding mode control and high-gain nonlinearity compensation for dual-motor driving system," *IEEE Trans. Ind. Inform.*, vol. 16, no. 6, pp. 4090–4098, Jun. 2020.

[12] S. G. Robertz et al., "Precise robot motions using dual motor control," in *Proc. IEEE Int. Conf. Robot. Automat.*, 2010, pp. 5613–5620.

[13] L. Sun, X. Li, L. Chen, H. Shi, and Z. Jiang, "Dual-motor coordination for high-quality servo with transmission backlash," *IEEE Trans. Ind. Electron.*, vol. 70, no. 2, pp. 1182–1196, Feb. 2023.

[14] B. Wang, M. Iwasaki, and J. Yu, "Command filtered adaptive backstepping control for dual-motor servo systems with torque disturbance and uncertainties," *IEEE Trans. Ind. Electron.*, vol. 69, no. 2, pp. 1773–1781, Feb. 2022.

[15] A. Khorasani et al., "A methodology for designing a lightweight and energy-efficient kinematically redundant actuator," *IEEE Robot. Automat. Lett.*, vol. 7, no. 4, pp. 10786–10793, Oct. 2022.

[16] M. Calvini, M. Carpita, A. Formentini, and M. Marchesoni, "PSO-based self-commissioning of electrical motor drives," *IEEE Trans. Ind. Electron.*, vol. 62, no. 2, pp. 768–776, Feb. 2015.

[17] J.-F. Shi, X.-F. Gou, and L.-Y. Zhu, "Calculation of time-varying backlash for an involute spur gear pair," *Mechanism Mach. Theory*, vol. 152, 2020, Art. no. 103956.

[18] M. Slamani, A. Joubair, and I. A. Bonev, "A comparative evaluation of three industrial robots using three reference measuring techniques," *Ind. Robot: Int. J. Robot. Res. Appl.*, vol. 42, no. 6, pp. 572–585, 2015.